

CFD-PBE SIMULATION FOR AN INDUSTRIAL GRANULATION PROCESS WITH SCREENING-CRUSHING

Philipp LAU¹, Zhen LI¹, Matthias POTTHOFF² and Matthias KIND^{1*}

¹ Institute of Thermal Process Engineering, Karlsruhe Institute of Technology, GERMANY

² Uhde Fertilizer Technology B.V., NETHERLANDS

*Corresponding author, E-mail address:matthias.kind@kit.edu

ABSTRACT

Fluidized bed spray granulation is applied in industrial scale, which is built up by connecting several granulation chambers in series using dividing walls and many nozzles, to produce granulate materials with a tailored particle size distribution. This size distribution can be obtained by a screening-crushing process after the granulators. The granules larger than the desired product size are crushed and fed back to the process together with the undersized granules. The aim of the development is to minimize the reflux after the sieve. Due to the large number of nozzles in a chamber and the large dimension of such a device, a granulator cannot be described completely using a numerical simulation. Hence, a “limited” 3D-model is developed to extract the exchange streams between two chambers as a function of various parameters, e.g. bed height, particle size etc.. In this investigation the smallest unit, which contains two fluidized beds divided by a slotted wall, is brought into focus. A spray nozzle is located in the center of each fluidized bed. Using Two Fluid Model (TFM) the reflux ratio of the particle streams between these two simulated fluidized beds is generated. The simulated reflux ratio is applied into a flow sheet simulation program “SolidSim” to obtain the streams in the entire process with four granulation chambers for a steady case by considering the population balance equations (PBE) and the Screening- Crushing process.

NOMENCLATURE

α	exponent of Plitt's equation	[-]
α	volume fraction	[-]
a	area of slot	[m ²]
b	fraction of bypass-particles	[-]
C_B	Bond Work Index	[kWh/t]
C_D	drag coefficient	[-]
$C_{fr,sp}$	coefficient of friction	[-]
d	particle diameter	[m]
e_{sp}	restitution coefficient	[-]
$g_{0,sp}$	radial distribution function	[-]
G_L	growth rate	[m/s]
G	elasticity modulus	[N/m ²]
K_{sg}, K_{sp}	exchange coefficient	[-]
\bar{m}	mean mass flow density	[kg/m ² /s]
\dot{M}	mass flow rate	[kg/s]
N_i	number of particles i	[-]
n	total number of meshed elements	[-]
P_s	solids pressure	[Pa]

ρ_s	density of particles	[kg/m ³]
Re_s	particle Reynolds number	[-]
Δt_n	time step	[s]
T	separation efficiency	[-]
μ_f	shear viscosity of fluid	[Pa·s]
v	velocity	[m/s]
\bar{v}_i	mean reflux ratio of particle phase i	[-]
W	specific work for reduction	[kJ/t]
x_{cut}	cut size	[m]
$x_{80,p}$	characteristic particle diameter	[m]

INTRODUCTION

Due to product properties, manageability and safety, granules are used in a wide range of industries (fertilizer production, food processing technology, chemical and pharmaceutical industry). One of the methods of producing granules is fluidized bed spray granulation, in which particles are fluidized in a chamber. Suspension or melting is atomized by a nozzle, so that drops can coat fluidized particles. The nozzle can be used as a top spray or bottom spray configuration. Due to the hot or cool fluidization air the solvent is evaporated or the coating solidifies and therefore particles grow. Besides experimental research numerical methods become more and more important to optimize the processes economically. The Two Fluid Model (TFM) has been shown as a possible method to consider a gas/solid suspension with a large number of particles (Gidaspow, 1994). In this method the gas phase and particle phase are treated as penetrated continua. The characteristic parameter of the particle phase is the volume fraction α . The interaction between particles (s) and air (g) can be described with the model of Gidaspow (1994). He combined the two models of Ergun (1952) and Wen & Yu (1966):

For $\alpha_g > 0.8$:

$$K_{sg} = \frac{3}{4} C_D \frac{\alpha_s \alpha_g \rho_g |\vec{v}_s - \vec{v}_g|}{d_s} \alpha_g^{-2.65} \quad (1)$$

For $\alpha_g < 0.8$

$$K_{sg} = 150 \frac{\alpha_s (1 - \alpha_i) \mu_g}{\alpha_g d_s^2} + 1,75 \frac{\rho_g \alpha_s |\vec{v}_s - \vec{v}_g|}{d_s} \quad (2)$$

The drag coefficient C_D is a function of Re_s and can be calculated with different equations. In the case of the existence of more than one particle phases, the interactions

between particles (phase *s* and *p*) are modeled with the equation of Syamlal and O'Brien (1987).

Granulators for large-scale granulation consist of several chambers and many nozzles (Fig 1). For CFD-simulation it is impossible to take all chambers and nozzles into account. Thus, a method has been developed to simulate the complete process with acceptable effort.

Firstly a spraying nozzle model is developed to get high-resolution results for the flow behind the orifice. Thereafter the velocity vector is applied into the "limited" 3D-model as a boundary condition for the granulation chambers. The reflux ratio between two chambers is generated from the specific mass flow densities of each particle phase, which are calculated with user defined functions. Then, the reflux ratio is applied into the population balance equations with the Screening-Crushing process using flow sheet simulation program "SolidSim".

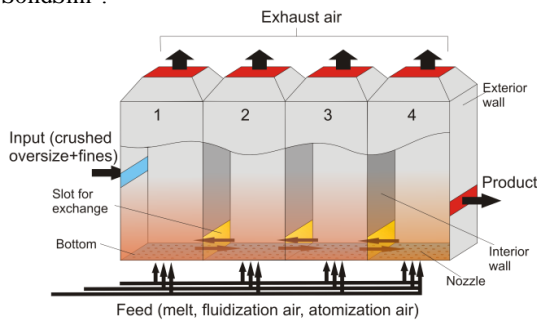


Figure 1: Model of a large-scale granulator with 4 chambers.

MODEL DESCRIPTION

"Limited" 3D-model

Due to the large velocity gradient in the zone near the nozzle, the mesh in this zone is extremely fine. It leads to a large number of cells for the simulated domain. Therefore it is not possible to compute the entire granulator. Fig. 2 shows the high number of nozzles on the bottom of two chambers. The chambers are divided by a slotted wall and interconnected by a slot, where particles can exchange between chamber 1 and chamber 2. Every chamber can be divided into unit cells, which have the same size and include only one nozzle in the middle of each cell.

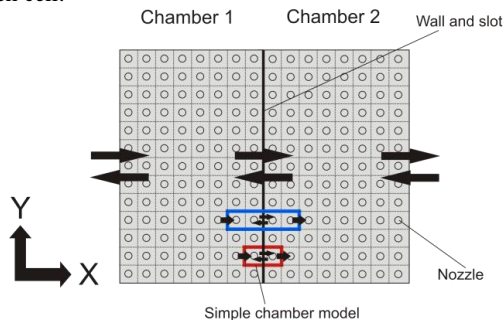


Figure 2: Schematic geometry of two granulation chambers and the developed chamber models.

To obtain information of exchange streams between chamber 1 and chamber 2, the region near the dividing wall and the slot is crucial. Every chamber can be considered as a continuous stirred-tank reactor (CSTR). Due to the inordinate motion of particles, the temporal

averaged volume fraction of particles (phase *i*) is constant. A boundary layer near the slot could be the reason for a profile change and for the exchange of particles (Fig. 3). Therefore a simple "limited" 3D-model is developed (red box, Fig. 2), which consists of two unit cells divided by a slotted wall. Additionally, a model containing four unit cells (blue box, Fig. 2) is studied. If there is no difference regarding to the reflux ratio, the number of nozzle rows will have no influence on exchange streams and the chamber model can be used for simulating the large-scale granulator.

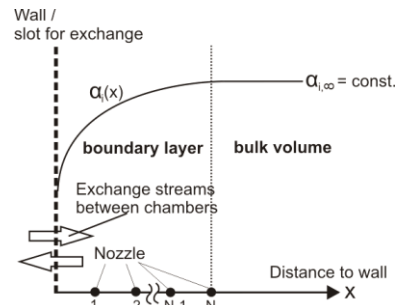


Figure 3: Boundary layer and exchange streams.

For this purpose a very simple chamber model was developed at first. It includes only 2 unit cells without nozzles, which are closed to environment. Dimensions of the "limited"-3D-model are shown in Fig. 4. Both chambers are interconnected by the yellow colored slot. The quadratic bottom of each chamber is $0.3 \times 0.3 \text{ m}^2$. The slot has a height of 0.1 m .

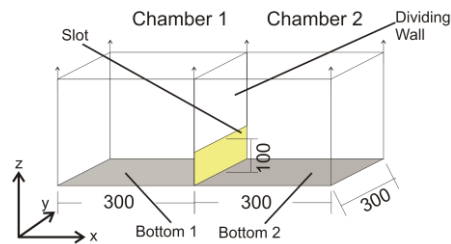


Figure 4: Dimensions (in mm) of the simple chamber model without nozzles.

The chambers are designed in Gambit. Because of the simple geometry (without nozzles) a structured mesh is used (Fig. 5).

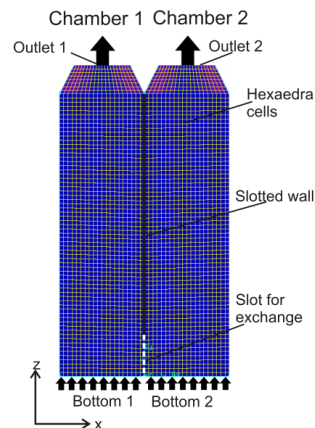


Figure 5: Simple chamber model without nozzles, $n = 120.000$.

The bottom of each chamber is defined as a mass-flow-inlet boundary condition. At the top of each chamber, a pressure outlet boundary condition is defined. To avoid reversed flow in the top of the chamber, the chambers have small outlets for directed flow. The chambers are divided by the slotted wall.

Another mesh has been designed to simulate the chamber model with nozzles. Fig. 6 shows the dimensions of the chamber model. The distance between nozzle and slotted wall is 0.15 m.

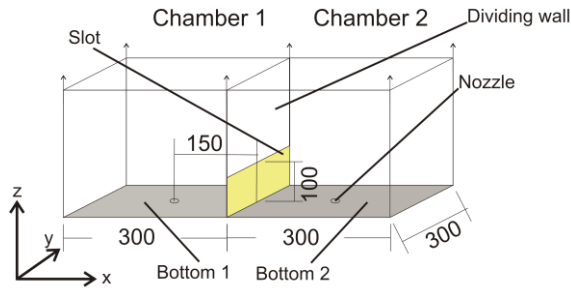


Figure 6: Dimensions (in mm) of the simple chamber model with nozzles.

To realize an acceptable aspect ratio of cells around the nozzle boundary condition, a method of hemispheres was used (Fig. 7). In addition to the boundary condition for fluidization air, a mass-flow-inlet for the nozzle air is used. External faces are defined as a stationary wall for the simple “limited” 3D-model. The advanced open chamber models are extended with a separate mass-flow-inlet and a pressure outlet for particles.

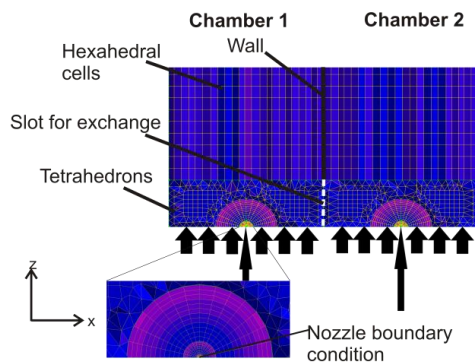


Figure 7: Using hemispheres for meshing the chamber model with nozzles, $n = 128.662$.

To obtain the influence of particle size, two different particle phases have been defined. Before running the simulation, each particle phase is filled into a chamber. After that, the simulation can be started. The slot is still closed and particles are fluidized. After 10 seconds simulated process time, the slot is opened and particles can exchange. Tab. 1 and Tab. 2 show the general settings for the numerical simulation and settings for the granular phases and the models used for calculation.

Mode of calculation	Transient
Time step	0.00001 – 0.001s
Multi-phase-model	Euler implicit
Turbulence model	Dispersed Reynolds-Stress-Model, linear

Interaction between phases	Gidaspow and Syamlal & O'Brien
Process temperature	110°C
Energy equation	no
Gravity acceleration	-9.81 m/s ²
Boundary condition orifice:	$v_{ax} = 160.10 \frac{m}{s}$ $v_{rad} = 11.09 \frac{m}{s}$ $v_{tang} = 88.47 \frac{m}{s}$
Computation of pressure	SIMPLE-algorithm
Discretization	First-Order-Upwind
Particle sizes	$d_{p2} = 1mm$ $d_{p1} = 2mm$

Table 1: General settings in ANSYS Fluent for simulating the “limited” 3D-model.

Characteristic of granular phase	Computational model
Granular viscosity	Gidaspow (1994)
Granular bulk viscosity	Lun et al. (1984)
Frictional viscosity	neglected
Granular temperature	Algebraic
Solids pressure	Lun et al. (1984)
Radial distribution	Lun et al. (1984)
Elasticity modulus	$G = \frac{\partial P_s}{\partial \alpha_s}, G > 0$
Packing limit	0.63; constant
Restitution coefficient	0.9; constant

Table 2: Settings for characteristics of granular phases.

Population balance model in “SolidSim”

The large-scale granulation process is shown in Fig. 8. Particles are granulated in four chambers and after passing the outlet of the last chamber they are cooled down in the first stage cooler. After that, the granules are classified in a screen with two screen decks. Particles with desired product size distribution are discharged. Particles, which are too large for the product stream, are fed back into chamber 1 (after size reduction in a crusher). Particles smaller than the product are directly fed back to chamber 1.

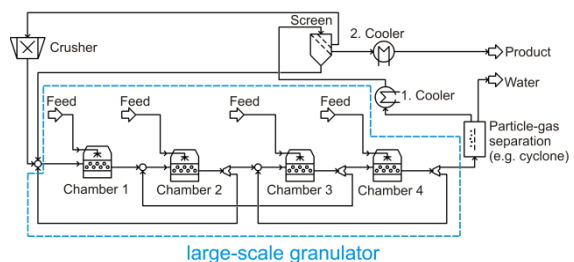


Figure 8: Schematic diagram of geometry.

The model of the large granulator contains four chambers and is shown in Fig. 8 (also see Fig. 1). To formulate a mean reflux ratio between chambers, splitter and mixing elements have been added to the flow sheet. Each chamber can be considered as a CSTR. Combining population balance equation (PBE) for steady case and the CSTR model, results in an equation for calculating the number of particles in each class i in a chamber (Mörl, 1980):

$$N_i = \frac{\frac{G_L}{d_p} N_{i-1} + N_{in,i}}{\frac{G_L}{d_p} + \frac{\dot{M}_m + \dot{M}_k}{m_{bed}}} \quad (3)$$

With \dot{M}_m being the mass flow rate of melt. The surface-dependent growth rate G_L can be calculated as follows:

$$G_L = \frac{2 \cdot \dot{M}_m}{A_{bed} \cdot \rho_s} \quad (4)$$

The general settings for the simulation of the large-scale granulation process are shown in Tab. 3:

Mode of calculation	Steady
Number of chambers	4
Particle bed mass in each chamber	1000 kg
Process temperature	110 °C
Chamber model	CSTR
Feed mass flow rate of urea	11.57 kg/s
Composition of feed stream	97-wt-% urea 3-wt-% water
Number of particle classes	500

Table 3: General settings for the flow sheet simulation.

The classification in the screen can be calculated with Plitt's model (1971). For each particle class the following equation is used:

$$T(x_i) = (1-b) \cdot \left(1 - e^{-0.693 \cdot \left(\frac{x_i}{x_{cut}} \right)^a} \right) + b \quad (5)$$

The settings for the screen can be seen in Tab. 4:

Number of screen decks	2
Model for classification	Plitt (1971)
Cut size 1 st stage	3 mm
Separation sharpness 1 st stage α	8
Cut size 2 st stage	2 mm
Separation sharpness 2 st stage	8

Table 4: General settings for the screen

The particle size distribution after the crusher can be calculated with the Bond equation (Stieß, 1994). In this correlation the required work for particle size reduction is inversely proportional to the square root of the particle size of the product:

$$x_{80,p} = \frac{1}{\left(\frac{W}{10 \cdot C_B} + \frac{1}{\sqrt{x_{80,f}}} \right)^2} \quad (6)$$

The settings for the screen can be seen in Table 5. The Bond Work Index C_B provides a measure of how much energy is required to reduce a unit weight from a theoretical infinite size to 80 percent passing 100 μm . It can be determined experimentally from laboratory crushing and grinding tests.

Crushing model	Bond
Mass specific power	4000 kJ/t
Bond Work Index C_B	12 kWh/t
Kind of grinding	dry
Particle size distribution of product	RRSB
Distribution coefficient n	5

Table 5: General settings for the crusher.

RESULTS

Closed "limited" 3D-model without nozzle

To obtain information about the reflux ratio between two chambers, the mass flux density out of and into a chamber of each particle phase ($d_{p1} = 2\text{mm}$, $d_{p2} = 1\text{mm}$) is important. For three different initial bed heights (100, 200, 300 mm) the allocation of masses of each particle phase is shown in Fig. 9. Particles are fluidized the first 10 seconds with closed slot. Thereafter, the slot is opened and particles can exchange between the chambers. With increasing bed height, required time to balance the mass of each particle phase in both chambers increases. Two effects lead to mass transportation into the opposite chamber. Firstly bubbles in the fluidized bed influence the mass transport through the slot. Small fluctuations shown in Fig. 7 occur because of mass transportation in bubbles and because of bubble break up. Secondly larger fluctuations of particle mass (e.g. 200 mm bed height) result from pressure compensation between chambers in analogy to two communicating pipes.

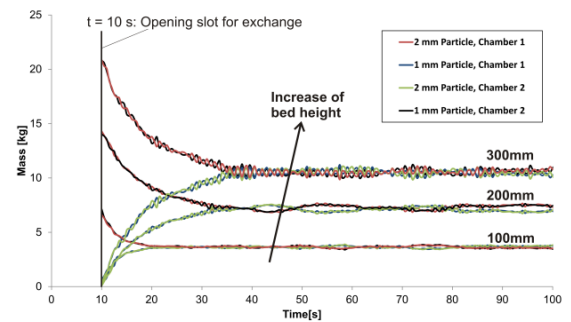


Figure 9: Exchange of mass for different bed heights.

The current mass flux density is defined as the mass flow rate of the sort of particles i at the time t_n divided by the surface of the slot, where particles can exchange:

$$\dot{m}_i(t_n) = \frac{\dot{M}_i(t_n)}{A} \quad (10)$$

A user defined function exports the mass flux density of entering and leaving particles to a txt-File at each time step. The temporal development of the mass flux density is shown in Fig. 10. To show the results clearly the entering particle stream is declared to be negative, the leaving stream to be positive.

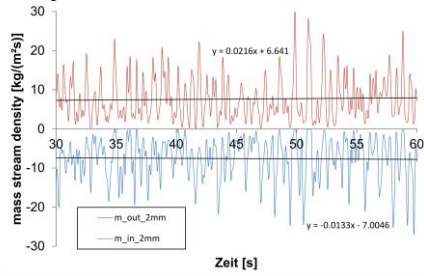


Figure 10: Mass flux densities for 2 mm particles at a bed height of 100 mm.

For a quasi-steady case, the mean mass flux density for entering and leaving particles of the phase i can be calculated in the following way:

$$\bar{\dot{m}}_{in,i} = \sum_n^N \frac{\dot{M}_{in,i}(t_n) \cdot \Delta t_n}{A \cdot \Delta t_{total}} \quad (7)$$

$$\bar{\dot{m}}_{out,i} = \sum_n^N \frac{\dot{M}_{out,i}(t_n) \cdot \Delta t_n}{A \cdot \Delta t_{total}} \quad (8)$$

The mean reflux ratio of each phase is then defined as

$$\bar{v}_i = \frac{|\bar{\dot{m}}_{in,i}|}{\bar{\dot{m}}_{out,i}} \quad (9)$$

For two chambers, which are only connected to each other and isolated from the environment, the mean reflux ratio trends to 1.

$$\lim_{t \rightarrow \infty} \bar{v}_i = 1 \quad (10)$$

Particles have to change between the chambers because there is no external force, which keeps an imbalance in the chambers. For long times the mean mass flux densities $\bar{\dot{m}}_{in,i}$ and $\bar{\dot{m}}_{out,i}$ have the same values. The mass flux densities of each phase are shown in Tab. 5 for the simple chamber model without nozzles.

	$d_{p1} = 2\text{mm}$	$d_{p1} = 2\text{mm}$	$d_{p2} = 1\text{mm}$	$d_{p2} = 1\text{mm}$
	$\bar{\dot{m}}_{in,i}$	$\bar{\dot{m}}_{out,i}$	$\bar{\dot{m}}_{in,i}$	$\bar{\dot{m}}_{out,i}$
bed height				
100 mm	-7.55	7.59	-7.58	7.61
200 mm	-13.72	13.8	-11.43	11.58
300 mm	-22.51	22.52	-19.77	19.68

Table 6: Mass flux densities for each particle phase for the simple chamber model without nozzles.

Considering Table 6, larger particles have a higher mass flux density than smaller particles. With the same mass flow rate of fluidizing air, smaller particles ($d_{p2} = 1\text{mm}$) usually exist in the upper part of the chamber and larger particles ($d_{p1} = 2\text{mm}$) gather at the bottom of the chambers. The segregation leads to a higher exchange intensity of larger particles, because the slot is located near the floor of the chambers. Figure 11 shows the average

volume fraction for 30 seconds and emphasizes the effect of segregation of particles.

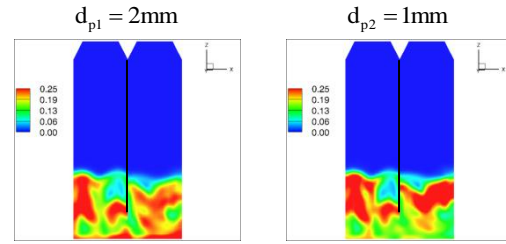


Figure 11: Average of particle volume fraction for 30 seconds.

Closed “limited” 3D-model with nozzle

The mass flux densities for different bed heights in this case are listed in Tab. 7. Comparing Tab. 6 and Tab. 7, the impulse of the nozzle air increases the transportability of particles, i.e. the nozzle intensifies the mass flux density through the slot.

	$d_{p1} = 2\text{mm}$	$d_{p1} = 2\text{mm}$	$d_{p2} = 1\text{mm}$	$d_{p2} = 1\text{mm}$
	$\bar{\dot{m}}_{in,i}$	$\bar{\dot{m}}_{out,i}$	$\bar{\dot{m}}_{in,i}$	$\bar{\dot{m}}_{out,i}$
bed height				
100 mm	-9.33	9.03	-8.67	8.55
200 mm	-20.34	20.53	-18.58	18.59
300 mm	-27.27	27.85	-24.25	25.6

Table 7: General settings for the crusher.

All in all, the results of the numerical investigation are illustrated in Fig. 12. With increasing of bed height, the intensity of exchange also increases.

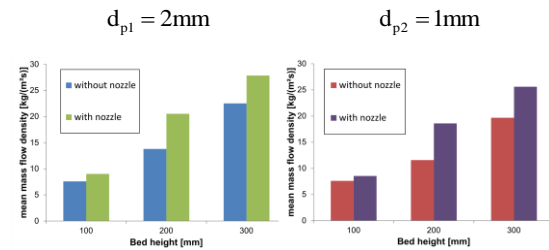


Figure 12: Summary results for the mean mass flow density.

Open “limited” 3D-model with nozzle

For real large-scale granulator applications the continuous process is characterized by external particles, which move through the chambers. For this reason, the geometry was changed by adding two more boundary conditions, namely the mass flow inlet and pressure outlet (Figure 13).

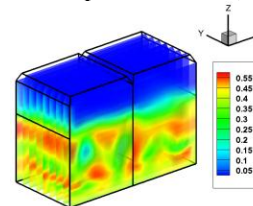


Figure 13: Open “limited” 3D-model with 2 chambers and 2 nozzles colored by volume fraction of particle phase.

Hence, it is possible to fill additional particles in the chamber. A pressure outlet guarantees that particles can leave the chamber. For the open chamber model only one kind of particle ($d_{p1} = 2\text{mm}$) was analyzed. The mean reflux ratios are shown in Fig. 14 for different mass flow rates of external particles at an initial bed height of 200 mm.

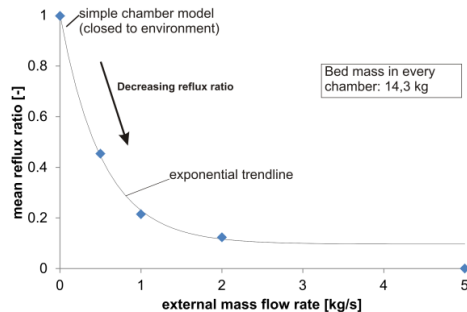


Figure 14: Mean reflux ratio as a function of external particle mass flow rate.

The closed chamber model (no external mass flow rate of particles) leads to a mean reflux ratio of 1. With increasing the mass flow rate of external particles the mean reflux ratio decreases. An exponential function is fitted to the first 4 points. At 5 kg/s there is no reflux stream back to the first chamber. The forced convection, caused by the mass flow rate of external particles, is too high for a reflux stream of particles.

A case with 4 unit cells in a row is also simulated for a mass flow rate of external particles of 1 kg/s. The mean reflux ratio is the same as in the case with two unit cells, 0.21. In this case the number of unit cells and nozzles has no influence on the reflux ratio. Thus, a reflux ratio of 0.21 is used for the PBE simulation in “SolidSim”.

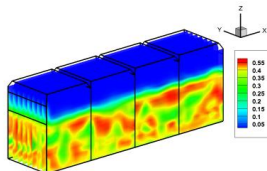


Figure 15: Open “limited” 3D-model with 4 chambers and 4 nozzles coloured by volume fraction of particle phase.

PBE simulation in “SolidSim”

The particle size distribution for a steady simulation in each chamber is shown in Fig 16. During the granulation process, particles grow in the chambers and therefore q_3 -distribution moves to the right during process, because a CSTR-model is used and a reflux ratio of 0.21 is considered.

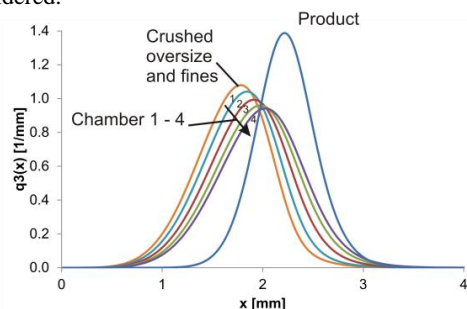


Figure 16: Volume fraction of particle phase, mean reflux ratio is the same for the 2-chamber and 4-chamber model.

Figure 17 shows that the q_3 -distribution becomes wider with an increasing mean reflux ratio. A reduced reflux ratio is desired to achieve a narrow product particle size distribution. This can be obtained by increasing the mass flow rate of the external particles.

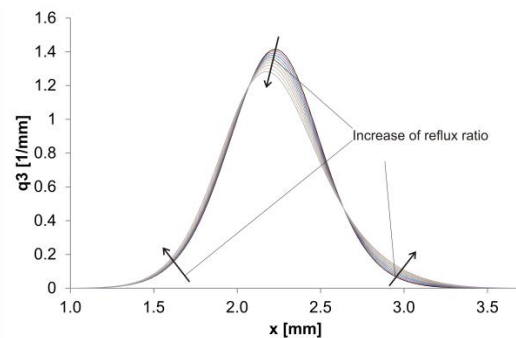


Figure 17: Volume fraction of particle phase, mean reflux ratio is the same for the 2-chamber and 4-chamber model.

CONCLUSION

In this investigation a method was developed to simulate an industrial large-scale fluidized bed spray granulation process using a combination of CFD and PBE. To obtain information about the reflux ratio in the complete process, a unit cell including a nozzle is brought into focus. Using the simulation of the “limited”-3D model, the mass flow rates of the particle exchange are obtained. It is revealed from these simulations, that bed height and nozzle air influence the transportability. The simulated reflux ratio obtained by upgrading the model to an advanced chamber model with 4 unit cells is identical to the one with 2 unit cells. This independent reflux ratio is applied into a flow sheet simulation for steady case to generate the particle size distribution in each chamber.

REFERENCES

- ERGUN, S., Orning, A.A. (1952), Fluid Flow Through Packed Columns, Chem. Eng. Prog., **48**, 89-94.
- GIDASPOW, D. (1994), Multiphase Flow and Fluidization: Continuum and Kinetic Theory Description, Academic Press, New York
- HÖFFL, K., (1986), Zerkleinerungs- und Klassiermaschinen, Springer Verlag, Berlin
- LUN, C., & SAVAGE, S. (1984). Kinetic Theories for Granular Flow: Inelastic Particles in Couette flow and Slightly Inelastic Particles in a General Flow Field, Cambridge: Cambridge University Press.
- MÖRL, L., (1980), Anwendungsmöglichkeiten und Berechnung von Wirbelschicht-Sprühgranulationsanlagen; Technische Hochschule Magdeburg; Dissertation B
- PLITT, L.R. (1971), The analysis of solid-solid separations in classifiers, CIM Bulletin **64** (708), 42-47.
- STIEB, M., (1994), Mechanische Verfahrenstechnik 2, Springer Verlag, Berlin,
- SYAMLAL, M. (1987), The Particle-Particle Drag Term in a Multiparticle Model of Fluidization, National Technical Information Service, Springfield, VA, DOE/MC/21353-2373
- WEN, Y., YU, Y. (1966). Mechanics of fluidization, Chem. Eng. Prog. Symp. Series, **62**, 100-111